Reaction Chemistry & Engineering

ROYAL SOCIETY OF CHEMISTRY

PAPER

View Article Online
View Journal | View Issue

Cite this: *React. Chem. Eng.*, 2024, 9, 666

Microfluidic localized hydrogel polymerization enables simultaneous recording of neural activity and behavior in *C. elegans*†

Hyun Jee Lee, Julia Vallier and Hang Lu *

Monitoring an animal's brain activity during motion provides a means to interpret brain activity in the context of movement. However, it is challenging to obtain information about the animal's movement during neural imaging in the popular model organism *C. elegans* due to its small size. Here, we present a microfluidic tool to immobilize only the head region of *C. elegans* for simultaneous recording of neuronal activity and tail movement. We combine hydrogel photopolymerization and microfluidics to realize controlled head immobilization in a semi-continuous fashion. To optimize the immobilization process, we characterize the hydrogel polymerization under different experimental conditions, including under the effect of fluid flow. We show that the Damköhler number specifically defined for our reactive transport phenomena can predict the success of such photopolymerized hydrogels used for sample immobilization. In addition to simultaneous recording of neural activity and behavior in *C. elegans*, we demonstrate our method's capability to temporarily reconfigure fluid flow and deliver chemical stimuli to the animal's nose to examine the animal's responses. We envision this approach to be useful for similar recordings for other small motile organisms, as well as scenarios where microfluidics and polymerization are used to control flow and reaction.

Received 2nd October 2023,
Accepted 16th November 2023

DOI: 10.1039/d3re00516j

rsc.li/reaction-engineering

Introduction

In neuroscience, animals' brain activity during a course of action or response is often recorded and interpreted to understand how the brain functions. The animal's motion undertaken during brain functional imaging provides the context for which the brain activities can be interpreted in relation to movement. In the case of the model organism, *Caenorhabditis elegans* (*C. elegans*), such an approach can identify neuronal and genetic origins of the locomotive behavior.[1–6] The millimeter long nematode has a simple and well-characterized nervous system, which is uniquely advantageous for understanding the molecular and cellular bases of biological processes.[7,8] Because of its small size and fluorescence microscopy-based readout of neuronal activities, multi-neuronal imaging has been traditionally achieved in physically or chemically immobilized animals;[9,10] a mobile animal would readily escape the imaging field of view and introduce confounding motion artifacts.[11] However, the immobilized state of an animal makes it challenging for meaningful behavior to be observed during functional imaging. The unavailability of concurrent behavioral information can obscure the interpretation of neural activities that may be correlated with the animal's movement. Additionally, the absence or hindrance of motor execution can produce unnatural neuronal activities or impair the animal's normal cognitive functions by compromising the proprioceptive feedback received by the animal.[12,13]

In order to obtain behavior-correlated neural activities in *C. elegans*, neural imaging of freely moving animals has been pursued.[1] While the resulting neural activity traces can be interpreted in conjunction with locomotive behavior, imaging is greatly limited by the low magnification objective required to keep the animal in the microscopic field of view, effectively constraining the experiment to imaging single or well-resolved neurons.[14–16] Multi-neuronal imaging at higher magnification requires active tracking and advanced equipment, which are often incompatible with microfluidic operations that enable controlled manipulation of the animal's environment.[17,18] This is particularly problematic for stimulation experiments, in which temporally precise external stimuli must be delivered to the animal. To our knowledge, multi-neuronal imaging of a moving *C. elegans* specimen during microfluidic stimulation has not been realized and remains needed in order to generate a more complete and naturalistic context for the interpretation of neuronal activity.

School of Chemical & Biomolecular Engineering, Georgia Institute of Technology, USA. E-mail: hang.lu@gatech.edu

† Electronic supplementary information (ESI) available. See DOI: https://doi.org/10.1039/d3re00516j

To address this need, an accessible method to simultaneously record the neural activity and behavior in *C. elegans* is needed. One approach is by immobilizing the animal only at the head region, where the neural activity is recorded, and concurrently tracking the motion of its unconstrained tail. This is analogous to head-fixed neural imaging in mice, fruit flies, and zebrafish, in which the head fixation provides convenient monitoring of neural activities of moving animals with minimal noise and motion artifacts.[19–21] Additionally, coupling the head fixation method with microfluidics can offer controlled manipulation of the animal's environment and expand the set of experimental tools for *C. elegans* research.[9,10,22] For example, *C. elegans* head immobilization in a microfluidic device would enable the delivery of controlled chemosensory cues to the animal's olfactory system to examine the neuronal responses to specific odorous material.

In this paper, we combine hydrogel photopolymerization and microfluidics to realize semi-continuous partial immobilization of *C. elegans*. The UV light-activated hydrogel polymerization, which is fast, temporally controlled, and area-specific, is engineered in two steps for separate purposes. The first polymerized hydrogel temporarily reconfigures fluid flow in the microfluidic device to guide and properly position the animal. The second polymerized hydrogel immobilizes the anterior region of the animal for stable neuronal imaging. To serially image multiple worms in the same device for high throughput, we strategically utilize a hydrogel lock-release mechanism to secure the hydrogel in place temporarily and release it after imaging each animal. Because the structural integrity of the resulting hydrogel is important for successful immobilization of the animal, we optimize the composition and UV dosage of the polymerization and characterize the extent of the reaction for each condition. Additionally, we examine the extent of polymerization in a flowing prepolymer, which describes the second gelation, and define the dimensionless Damköhler number pertinent to the reaction. We demonstrate that the method enables the correlation of neural activities and behavior, comparison of neural activities in partially and fully

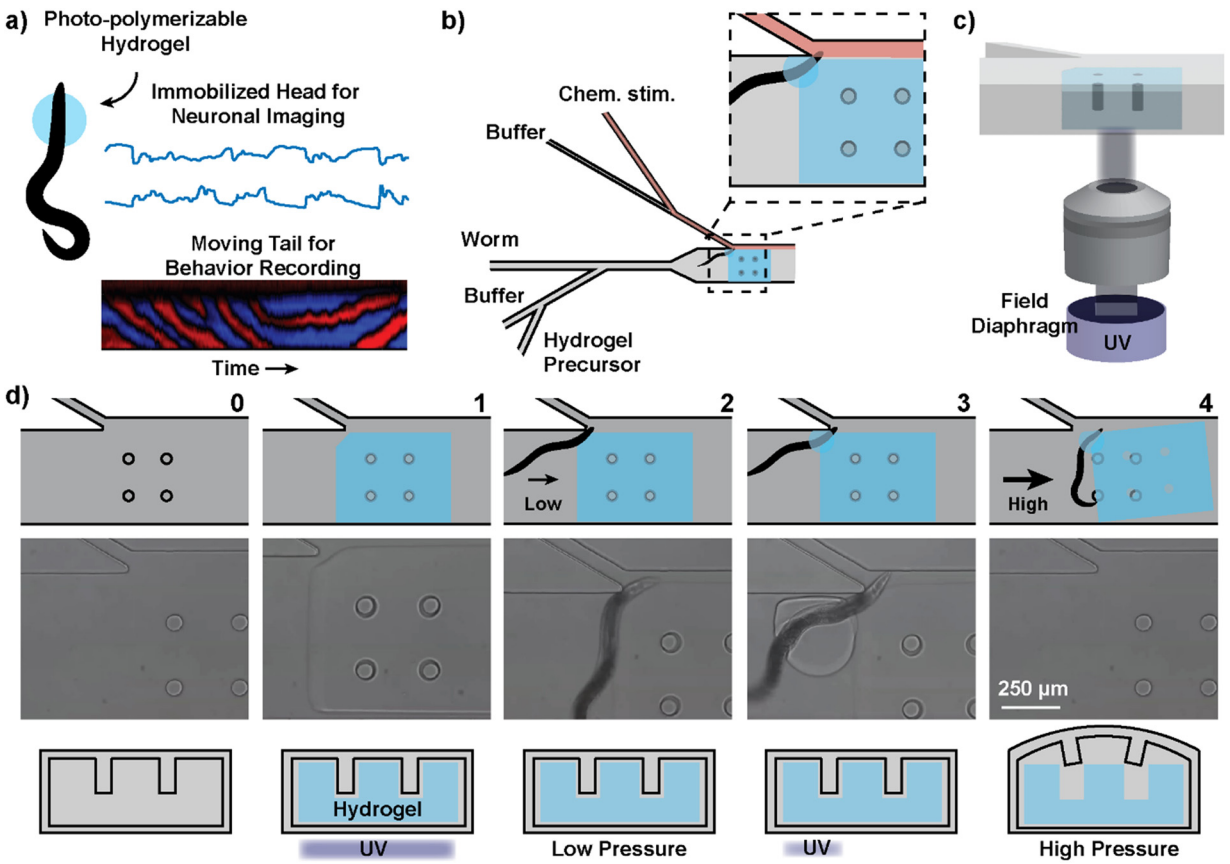

Fig. 1 Selective immobilization of *C. elegans* and the microfluidic implementation for multi-use capability. a) The photo-polymerizable hydrogel is used to selectively immobilize the animal's head for neuronal imaging while allowing its tail to move for behavior recording. b) The microfluidic device is designed to enable repeated uses of the hydrogel immobilization strategy and delivery of chemicals to the worm's anterior region. c) 3D view of the UV illumination through the field diaphragm to polymerize the hydrogel. d) Device operation in 4 steps: (1) a rectangular hydrogel block is polymerized over the pillars attached to the ceiling. (2) A worm is loaded and positioned at the gap using a low-pressure flow. (3) Lock: a second hydrogel is polymerized over the worm's anterior region and the existing hydrogel block. (4) Release: after recording, the worm and the hydrogel are released from the device by using a high-pressure flow, which deforms the PDMS ceiling and the pillars to allow sliding of the hydrogel.

immobilized animals, and imaging during chemical stimulation.

Results and discussion

Localized immobilization of the *C. elegans* head (or tail) using hydrogel photo-polymerization

In order to stabilize the site of neuronal imaging while allowing other parts of the animal to move freely, we used hydrogel photo-polymerization to immobilize a subsection of the *C. elegans* body. The anterior region of the animal is encapsulated by a hydrogel upon selective exposure of the prepolymer to UV. Immobilizing this region, where the neurons of our interest are concentrated, enables stable multi-neuronal imaging without tracking the worm's location (Fig. 1a). The prepolymer surrounding the posterior region of the animal is left unpolymerized such that the tail is free to move, and the movement can be monitored for behavioral analysis. Compared to previous methods of localized immobilization, such as using glue adhesives[23,24] or microfluidic vacuum,[25,26] the photopolymerizable hydrogel offers more control and flexibility over the area and timing of immobilization. The polymerization reaction has a sub-second speed and poses minimal risk to the animal's health at the selected wavelength (380–410 nm) and dosage of UV (0.5–2 J cm^{-2}).[27,28]

The polymerization chemistry and composition of the hydrogel were carefully selected considering several criteria. The reaction must be photoactivated to be area-specific and fast enough to immobilize actively swimming *C. elegans*. The physical properties of the polymerized hydrogel, such as its size and internal rigidity, should allow effective immobilization of the animal's target region for the duration of imaging. Lastly, the reagents should be non-toxic and have minimal effect on the worm's health. Based on these criteria, we identified free-radical polymerization of polyethylene glycol diacrylate (PEGDA) as an ideal polymerization chemistry for this application. PEGDA was chosen as the crosslinker due to its fast reaction speed and biocompatibility.[29,30] We selected lithium phenyl-2,4,6-trimethylbenzoylphosphinate (LAP) as the photoinitiator because it is water-soluble, has low cytotoxicity, and allows polymerization with visible light at 390 nm.[30] We determined that polymerizing a 30% PEGDA solution with light irradiation of wavelength 390 nm for 1 second at 796 mW cm^{-2} was sufficient to securely immobilize a worm's head region for at least 10 minutes. The size of the circular cross-section of the hydrogel, determined by an adjustable field diaphragm in the microscope, was approximately 200 μm in diameter. The animal experienced slow plasmolysis due to the hypertonic hydrogel precursor, but it remained active for the course of behavioral recording. When the animals in the precursor were recovered in buffer, they displayed normal movement comparable to those that had not been exposed to the hydrogel precursor (Fig. S1 and S2†).

Microfluidic implementation of hydrogel-enabled trapping and imaging

In addition to selectively immobilizing a portion of the *C. elegans* body, we designed a microfluidic method to enable chemical stimulation and continuous sequential imaging of immobilized animals (Fig. 1b). The delivery of chemical stimuli is achieved similar to that from the *C. elegans* stimulation device by Cho *et al.* that can deliver chemical stimuli with a temporal resolution of around 1 second.[10] Unlike the previous design, which restricts worm movement in a tight microchannel, we have a large chamber to allow for unrestricted tail movement.

To enable high-throughput imaging, we have adopted technological concepts from flow lithography, which is a microfluidic method to synthesize UV-patterned hydrogel microparticles in a continuous fashion.[31,32] For selective polymerization, the UV exposure is restricted to only the region of interest by using the field diaphragm of the microscope (Fig. 1c). The inhibition of free-radical polymerization near polydimethylsiloxane (PDMS) surfaces is leveraged to synthesize free-standing hydrogels that can be removed from the device. Because PDMS is oxygen permeable and oxygen inhibits free-radical polymerization, there exists a layer of unpolymerized prepolymer solution between the hydrogel and PDMS surface. The removability of the gel is important for continuous imaging of many animals in series because a hydrogel permanently bound to the device would prevent continued use of the same device for subsequent animals. Here, since we want to temporarily immobilize the hydrogel during imaging, we have added a lock-release mechanism that only releases the hydrogel above a critical pressure.[33] The locking is attained when the gel is polymerized encapsulating the pillar structures attached to the ceiling of the PDMS device (Fig. 1d-1). The polymerization proceeds around the pillars, creating a hydrogel block with small gaps that surround the pillars. The release is achieved only when the pressure within the device is sufficiently high to deform the PDMS ceiling and allow the hydrogel to slip past the deformed pillar structures (Fig. 1d-4).

Our microfluidic method involves two gelation processes within a four-step operation (Fig. 1d; ESI† Video S1). Taking advantage of the locking mechanism, we first construct a large rectangular hydrogel over the pillars that will temporarily reconfigure the fluid flow to guide the worm to the junction for chemical stimulus delivery (Fig. 1d-1). The rectangular hydrogel also serves as an anchor for the second hydrogel. Then, using a low-pressure reconfigured flow, the worm is loaded into the device and positioned at the junction (Fig. 1d-2). Once the worm is at the junction, a second gel (circular cross-section) is polymerized over the head region of the animal and the existing hydrogel wall (Fig. 1d-3). The result is a head-immobilized animal in a circular hydrogel that is attached to the temporarily stationary rectangular hydrogel. After imaging, a high-pressure flow (>45 psi)

releases the combined hydrogel and the worm together (Fig. 1d-4). This process can be repeated for many worms for high-throughput imaging.

Characterization of the fluid flow reconfiguration

In our design, the rectangular hydrogel block serves to both reconfigure the fluid flow to guide the animal toward the junction and anchor the second hydrogel. For the former purpose, the existence of the semi-solid hydrogel anchored to the PDMS ceiling diverts fluid flow around the hydrogel. The advantage is that this flow reconfiguration hydrodynamically steers *C. elegans* and aligns it for imaging and chemical stimulation. To characterize the flow reconfiguration with and without the temporary hydrogel block, we recorded the movement of beads (average diameter of 3 μm) under a flow (Fig. 2a and d) for particle image velocimetry analysis (experimentally measured velocity fields shown in Fig. 2b and e). The presence of the hydrogel block is effective in changing the flow streamlines and generating a flow velocity gradient and a focusing effect within the channel (Fig. 2e). With the hydrogel block, the increase in velocity toward the opened slit draws the swimming animal to the junction. The velocity profile along the transverse direction to the flow changes from somewhat parabolic to more linear in shape (Fig. 2c and f). While the convective flow inside the nano-porous hydrogel matrix is negligible,[34] there is still a flow around the top and bottom of the hydrogel because of the oxygen inhibition layers (approximately 8.5 μm based on reported reaction rates) near the PDMS. Similar hydrodynamic focusing was observed for all flow rates in the device operating range (0.1–8 mm s^{-1}). Beyond the application of hydrodynamic focusing to guide *C. elegans* loading, our result demonstrates that hydrogels can be generally used to temporarily change the channel structure and reconfigure fluid flow in PDMS microfluidic devices.

Characterization of the hydrogel polymerization

Once the animal is captured by the flow and the positioning of the hydrogel block, the circular hydrogel is synthesized to immobilize the animal under the fluid flow. We next characterized the polymerization of the circular hydrogel, whose structural integrity determines the effectiveness of worm immobilization. First, we indirectly examined the extent of the polymerization reaction by two methods: quantifying the size of the hydrogel cross-section and quantifying the average fluorescence signal of fluorophores conjugated in the hydrogel matrix.[35,36] The fluorescence intensity serves as a proxy for the internal density of the hydrogel.

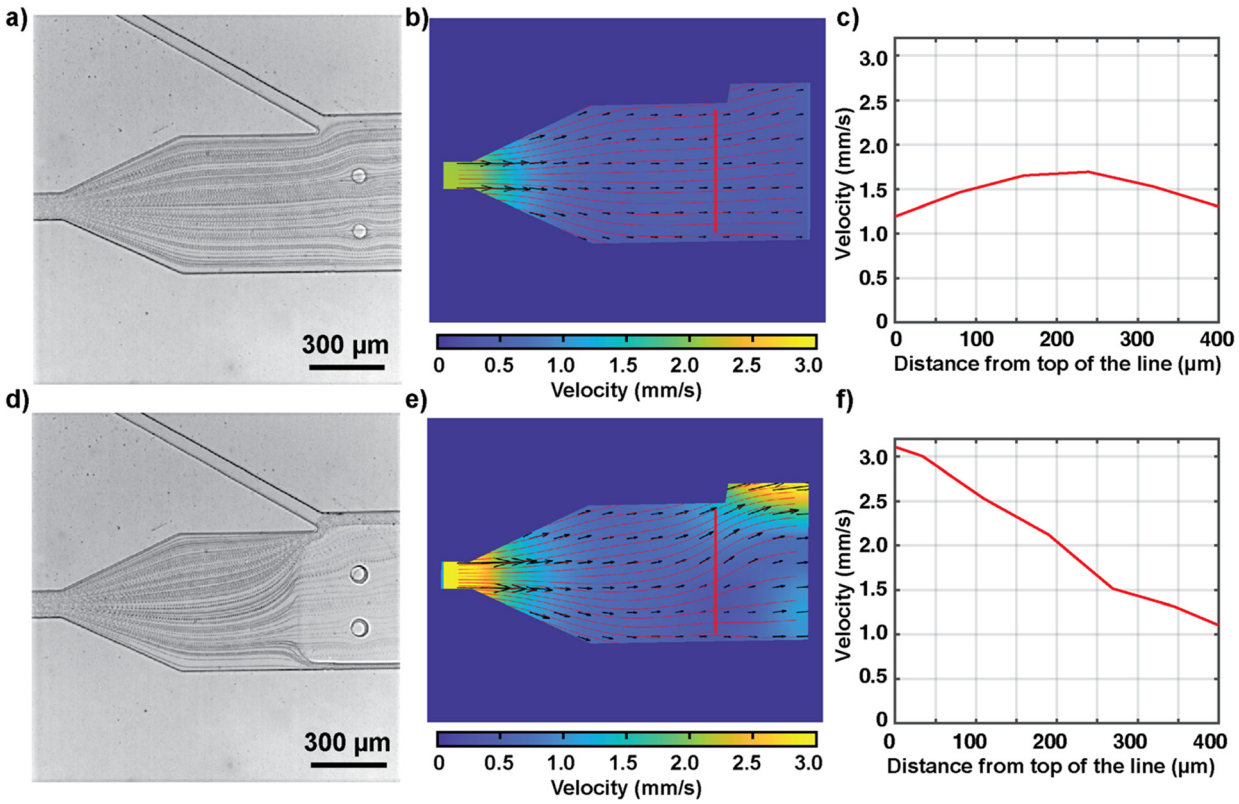

Fig. 2 Fluid flow reconfiguration upon creation of the temporary hydrogel wall. (a and d) Flow pathlines before (a) and after (d) gel polymerization visualized by combining high-speed images of the tracer particle flow. (b and e) Flow velocity vector streamlines and spatial profiles before (b) and after (e) gel polymerization. (c and f) Flow velocity profiles along the vertical line in panels b and e, respectively.

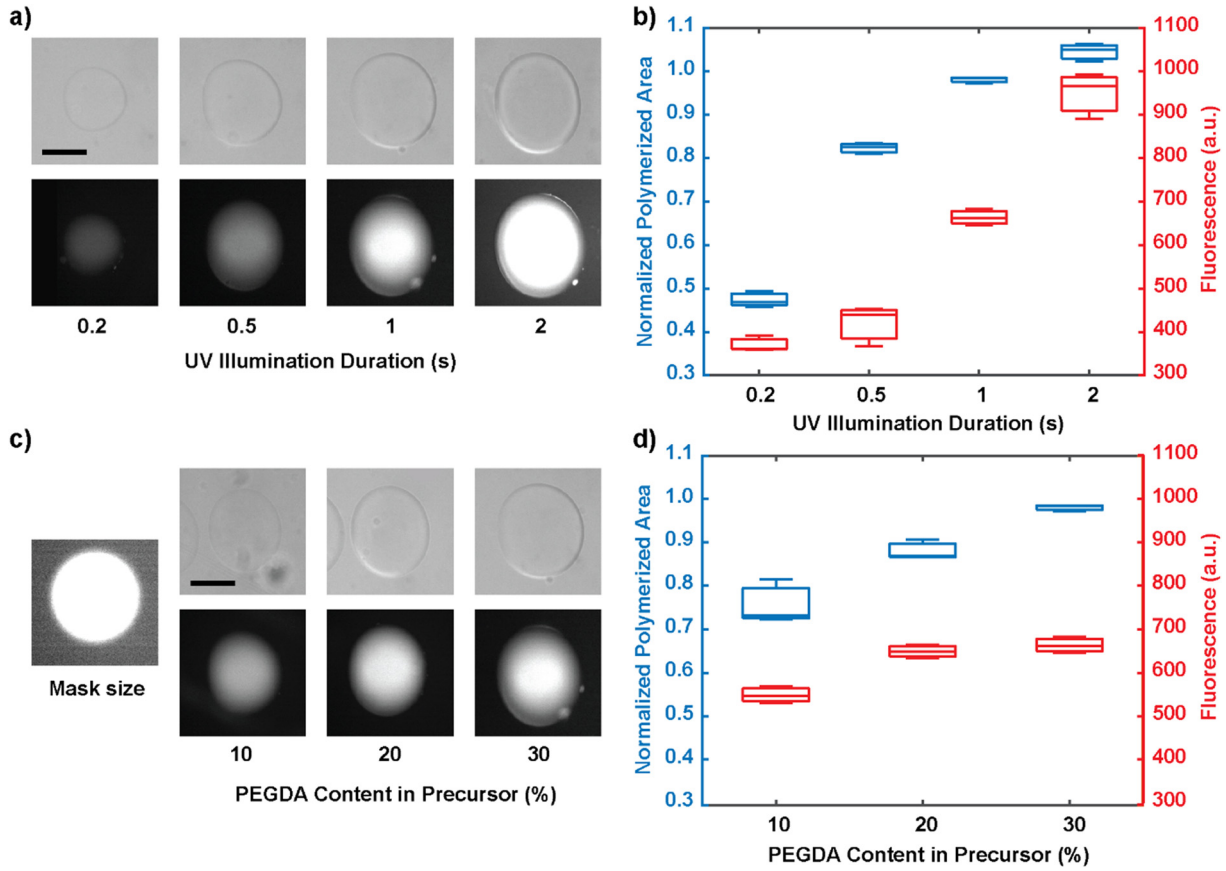

Fig. 3 Optimization and characterization of the gel polymerization in relation to UV dosage and crosslinker content. (a) Visual comparison of hydrogel size and fluorescence intensity by UV illumination duration. The fluorescence intensity indicates the crosslinking density of the hydrogel. (b) The effect of UV illumination duration on the cross-sectional area of polymerization (left axis) and the polymerization density indicated by signal of conjugated fluorophores (right axis). The area of the polymerized gel is normalized by the mask area. (c) Visual comparison of hydrogel size and fluorescence intensity by PEGDA content in the precursor. (d) The effect of percentage of PEGDA in the prepolymer solution on the cross-sectional area of polymerization (left axis) and the polymerization density indicated by the signal of crosslinked fluorophores (right axis). For each box plot in panels b and d, the central mark indicates the median, and the outline indicates the lower and upper quartiles. For each box plot, the center line indicates the median, and the bottom and top edges indicate the 25th and 75th percentiles, respectively. The whiskers indicate the most extreme data points that are not outliers. Scale bar: 100 μm.

As expected, as the duration of UV light illumination increases, the size of the hydrogel cross-section increases, reaching the mask size at 1 second and exceeding the mask size at 2-second exposure (Fig. 3a and b). With longer illumination times, the extent of the size increase plateaus. The initial increase in size beyond the size of the mask is likely due to diffusion of reactants; this effect reaches its maximum once the gel is largely crosslinked and the size does not increase indefinitely. Similarly, the crosslinking density also increases with the duration of UV illumination, but the extent of increase displays a different behavior: the density increases faster at higher UV dosages. This suggests that the polymerization reaction proceeds from the center of the hydrogel where oxygen depletion is reached first, and that the radial expansion of the reaction dominates the internal saturation at the initial stages; meanwhile, once the size of the gel has reached its mask size, the additional UV dosage is mainly absorbed to increase the internal crosslinking density. Practically, through experimentation, we determined that at least 1 second of UV exposure is required to achieve effective immobilization of the animal, and thus it was used for all subsequent experiments. Lastly, increasing the PEGDA concentration in the prepolymer solution also increases the extent of the reaction (Fig. 3c and d). PEGDA concentrations of 20% and 30% were both capable of capturing the animal, but 30% PEGDA resulted in more reliable and sustained immobilization.

Since the circular hydrogel must be polymerized under fluid flow conditions to keep the animal at the junction, we characterized the resulting gel sizes at different flow velocities (Fig. 4a–c). The flow velocity near the mask region was calculated using particle image velocimetry in the presence of the rectangular hydrogel wall, as discussed before. We tested flow rates that encompass the operating range, with the higher end bound by the high-pressure flow that releases the locked hydrogel. Empirically, to polymerize a gel that is at least 90 percent of the mask size, which is optimal for worm immobilization, a flow rate of around 0.5

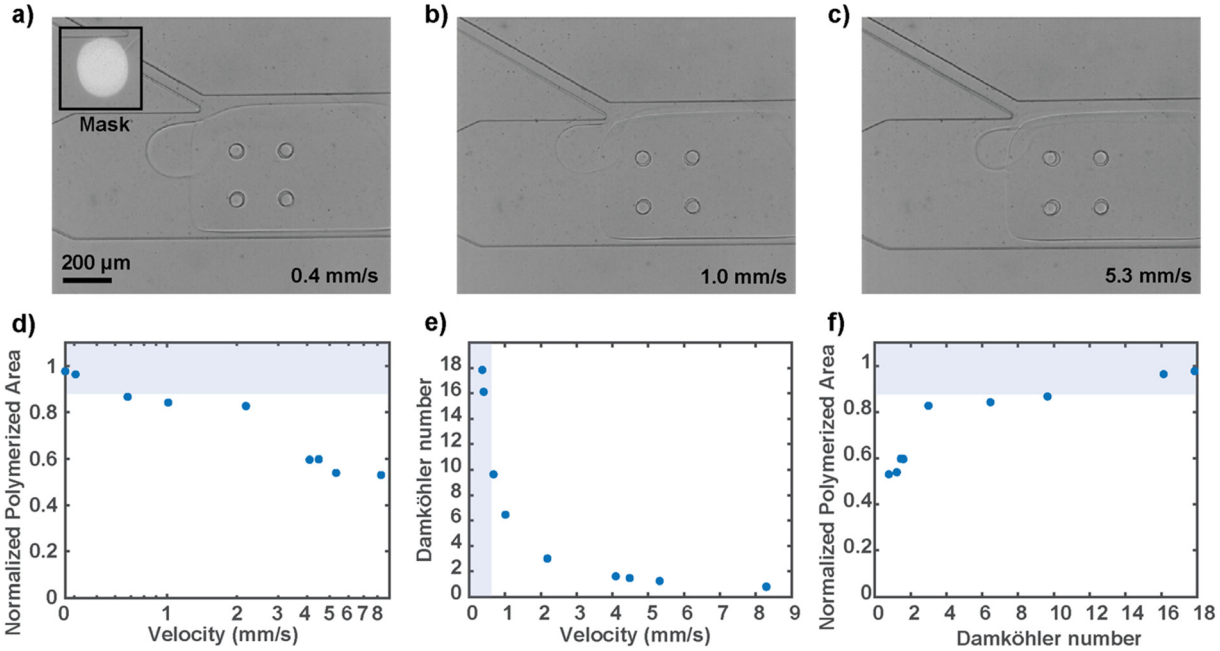

Fig. 4 Characterization of the extent of gel polymerization in a flowing prepolymer of different velocities. (a–c) Qualitative size comparison of circular hydrogel polymerized under different flow rates. (d) Flow velocity dependency of the extent of gel polymerization. The shaded region represents the operation conditions that result in a gel size of at least 90 percent mask size, which is optimal for worm immobilization. (e) Range of Damköhler numbers (comparing oxygen quenching rate to fluid flow rate) associated with the operating flow rates. (f) Relationship between the normalized area of gel polymerization and Damköhler numbers that relate the oxygen quenching rate to fluid flow rate.

mm s^{-1} or below is desired (Fig. 4d). A faster flow rate decreases the extent of the reaction because the fluid flow effectively replenishes the reaction-inhibiting oxygen, and therefore not enough free radical species are available to provide for substantial propagation of the free-radical polymerization. To overcome the reaction-inhibiting oxygen brought in by the flow, one would have to use higher UV illumination intensity or much longer illumination, neither of which is desirable for the present biological sample.

To generalize the competing relationship between the consumption and replenishing rate of the reaction-inhibiting oxygen, we defined the dimensionless Damköhler number that relates the rate at which oxygen is exhausted by the radicals to the rate at which oxygen is supplied by the convective flow (Fig. 4e). The expression of the dimensionless number was derived from the mass balance equation of oxygen and approximated with the assumption that the rates at which the radicals are generated and consumed are equal (ESI†). The simplified expression is as follows:

$$\mathrm{Da} = \frac{r_a L}{[O_2]_{eq} U_x}$$

where r_a is the rate of radical formation, L is the dimension of the UV mask, which is the relevant dimension of the reaction zone, $[O_2]_{eq}$ is the dissolved oxygen concentration, and U_x is the flow speed. We observed that the flow rates that resulted in a gel size of at least 90 percent mask size were characterized by Da $>$ 10 (Fig. 4f). Parameters used for the Damköhler number calculation are provided in the ESI† (Table S1). The qualitative observation of the gelation at all flow rates and the Damköhler number estimation reveal that the reaction-dominant regime is maintained for polymerization under a broad range of flow rates in our system. The Damköhler number analysis also provides a reference for application in other hydrogel polymerization chemistry and flow systems.

Simultaneous recording of behavior and neuronal activity

The primary purpose of the partial immobilization of the animals is to record their behavior and neuronal activities simultaneously. By polymerizing a hydrogel near the anterior region of a worm that is genetically modified to express the calcium indicator GCaMP in the neurons of our interest, we obtained images of both the neuron activities and the worm's behavior simultaneously (Fig. 5; ESI† Video S2). The worms were imaged on a standard epifluorescence microscope at 10× magnification, at which individual neurons can be distinguished while offering a large field of view to capture the animal's tail movements. Dual fluorescence recordings in green and red channels were used to extract ratiometric calcium transients of the neurons. The animal body's autofluorescence, which is prominent in the green channel, eliminated the need for a simultaneous brightfield recording. It should be noted that using a low-magnification objective necessitates a trade-off between field of view and spatial resolution; by gaining behavior readout, widefield

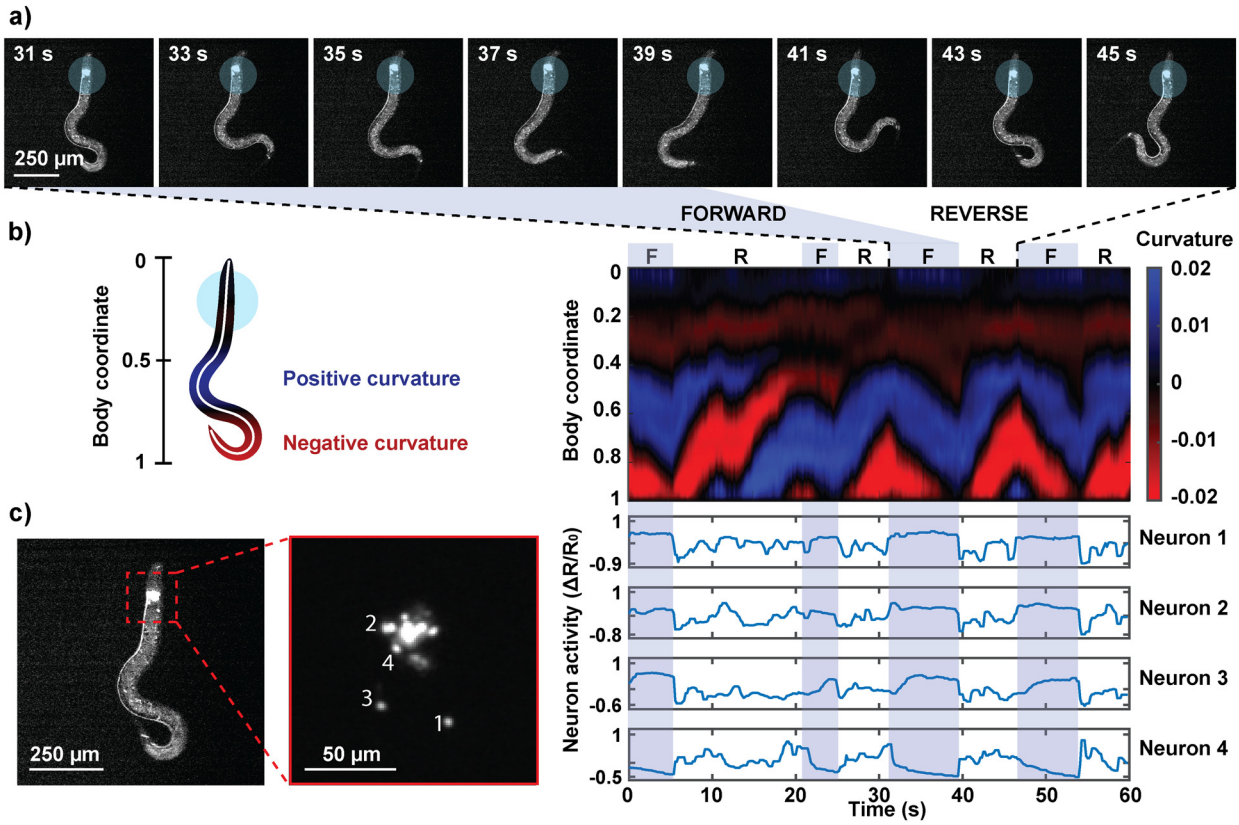

Fig. 5 Simultaneous recording of behavior and neuronal activities in head-immobilized *C. elegans*. a) Behavioral recording of a worm whose anterior region is immobilized in the hydrogel. The first five snapshots show a forward movement as defined by the wave propagation toward the tail. The last four snapshots represent a reverse movement. b) Behavior recording represented as a kymograph of worm centerline curvature. Forward and reverse movements are identified by the band slopes. c) Neuronal traces extracted from four head neurons that show movement-correlated calcium activities.

fluorescence microscopy in low magnification limits the resolvability and identification of neurons when neurons are too close to each other or outside the depth of field. As a result, we have focused our analysis on neurons that are in focus and well resolved. Engineering transgenes to express in a subset of head ganglion neurons could ensure that this is the case for other applications.

From the behavioral recordings, we observed and identified forward and reverse movements in the animals' semi-immobilized behavior (Fig. 5a). Forward or backward movements are characterized by a wave propagation in the head-to-tail or tail-to-head direction, respectively. The time course of the worm's behavior was represented as a kymograph of body curvature (Fig. 5b) to juxtapose the behavior and neuron activities to draw visual correspondence. The neurons were segmented and tracked in the red channel, and their signals were extracted in the green channel. Fig. 5c shows the ratiometric calcium activities of four neurons that exhibited motion-correlated activities. We observed that the activities of neurons 1, 2, and 3 are correlated with the worm's forward movements. Neuron 4, on the other hand, was activated during reversals and suppressed during forward motions. The capability to correlate the neuronal activities with the animal's concurrent behavior facilitates the identification of neurons that are motion-correlated, promoting a deeper understanding of otherwise seemingly spontaneous neuron activities.

The hydrogel photopolymerization also enables a unique experiment in which an individual worm's neural activities can be monitored in both the head-immobilized and full-body immobilized states. This is difficult to achieve in other microfluidic platforms because the device design typically only allows one type of immobilization, and animal recovery after imaging is not trivial. Our method can easily execute the two types of immobilization in series by imaging animals in partial immobilization followed by full-body encapsulation, which eradicates all behavior readout similar to conventional devices (Fig. 6a and b). The head region of an animal in the hydrogel precursor is first illuminated with UV through a smaller mask (circle diameter of 250 μm). After behavior-coupled neuronal imaging, the same animal is exposed to UV through a mask encompassing the entire body of the worm. This full-body immobilized animal can be flushed out of the microfluidic device with high pressure as with the head-immobilized animals. This unique series of imaging allows us to directly compare the activities of the same neurons in the same animal in either state of immobilization and interpret the effect of full immobilization

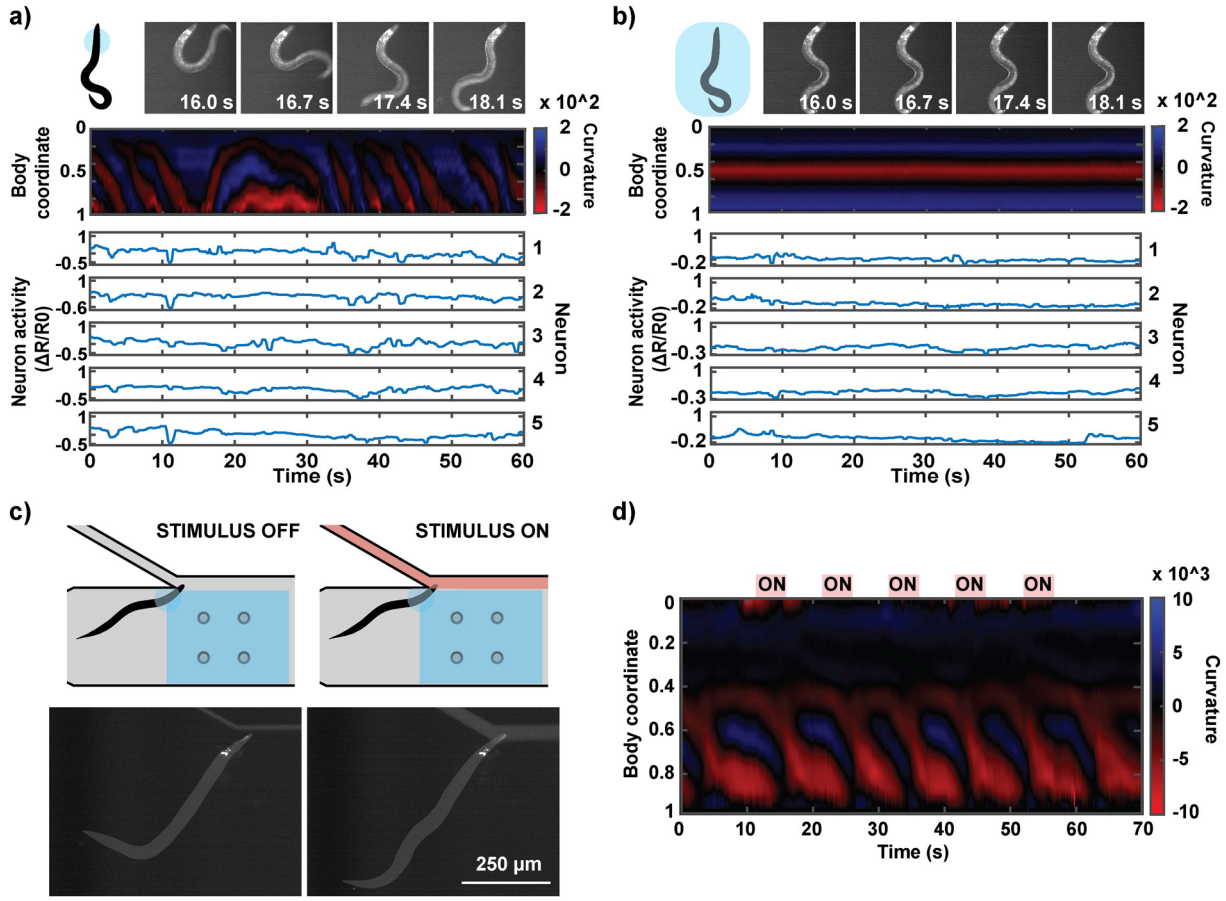

Fig. 6 Proof of concept experimental designs. Behavior and neuronal activities of a worm in partial-immobilization and whole-body immobilization. a) An animal's head is encapsulated with hydrogel before its whole body is immobilized with hydrogel. b) The worm fully encapsulated with hydrogel cannot display meaningful behavior. Simultaneous recording of behavior and neuronal activities in head-immobilized *C. elegans* during chemical stimulation. c) Pulses of chemical stimulants are delivered to the worm's anterior region. d) Body curvature kymograph. The red strips illustrate the time points during which the five 5-second pulses of isoamyl alcohol were delivered.

on an animal's neuronal activities. As observed by others, fully immobilized animals tend to have suppressed neural activities, suggesting that locomotion feedback is important for at least some parts of the neural circuits.

Fig. 6c demonstrates another application of the system where the partial immobilization of the animal allows for the delivery of defined chemical stimuli to the animal. Delivering temporally and compositionally precise chemical stimulation to a behaviorally active animal has not been achieved previously. The concurrent behavioral information during chemical stimulation offers interpretability of the animal's perception of the chemical stimulus. For this application, we designed our microfluidic device so that the immobilized region of the animal is placed at a junction at which a chemical stimulus can be delivered to the olfactory system (Fig. 6c). We confirmed that we can reliably deliver the stimulus at a temporal resolution of 1 s (Fig. S3†). We were able to deliver five 5-second stimulations of a known attractant (isoamyl alcohol) to a head-immobilized worm and acquire its behavioral information (Fig. 6d; ESI† Video S3).

Conclusion

In this work, we introduce a method to temporarily immobilize a selected region of *C. elegans* using a combination of hydrogel polymerization and microfluidics. Hydrogel photopolymerization in a PDMS device is engineered to achieve four functions: (1) temporarily reconfigure the fluid flow to load the animal to a specific region, (2) immobilize the head region of the animal with spatiotemporal specificity, (3) deliver chemical stimuli to the animal, and (4) remove the animal for high throughput operation of the device. For optimal hydrogel-based immobilization of the animal, we characterize the reconfigured flow patterns and velocity profiles and the extent of polymerization, with special regards to the effect of the fluid flow during the reaction. We demonstrate our method's utility in simultaneous recording of neuronal activity and behavior in *C. elegans*, investigating the effect of full-body immobilization on neural activity in an individual worm, and chemical stimulation of a tail-moving worm.

Our method has direct implications in *C. elegans* imaging. Simultaneous recording of neural activity and behavior enables the correlation of each neuronal activity trace to the behavior repertoire displayed by the animal during the same recording. This facilitates the identification of neurons whose activity corresponds with certain behavioral dynamics and therefore may be directly or indirectly involved in the locomotion output. At the neural circuit level, this allows us to gain a better glimpse of signal transmission from the sensory neurons to interneurons and motor neurons to produce the ultimate behavior. This can also provide interpretation of an individual animal's state of being or response to a stimulus. For example, a back propagation of curvature along the body length and curling generally signify the animal's aversion or attempts to escape the environmental cues. This can potentially eliminate the need to perform separate neuronal calcium imaging and behavior assays and resolve the fundamental limitations of comparing the neural and behavior data of two different populations.

Our work also has implications beyond *C. elegans* research. The immobilization approach is not limited to *C. elegans* but applicable to essentially any specimen, living or non-living, in the appropriate size range. The method offers great flexibility as the size and composition of the hydrogel can be tuned for specific needs. Furthermore, the approaches taken to engineer our tool are independently relevant to broader microfluidics and polymerization systems. The creation of temporary "walls" and reconfiguration of the flow may be useful for designing a microfluidic system that is adaptable to different sample sizes. It offers a way to redesign the microfluidic channel on demand without having to recreate the master PDMS mold. The characterization of the extent of the polymerization and the Damköhler number analysis, which revealed the operating bounds of our method, serve as guidelines to apply the approaches to other polymerization and flow systems.

Methods

Master fabrication and PDMS casting

A silicon wafer master with channels in high relief and pillars in counter relief was fabricated following the protocol by San-Miguel and Lu.[37] Two layers of SU-8 2050 (MicroChem) were developed onto the wafer: first, a 40 μm layer with no pillars in the imaging arena; then, an additional 50 μm layer with pillars. The master was silanized overnight with trichloro(1*H*,1*H*,2*H*,2*H*-perfluorooctyl)silane (Sigma-Aldrich). The device design features five inlets and an outlet. The two inlet channels for chemical stimulation have a width of 50 μm, and the other three inlet channels have a width of 100 μm. The pillars have a diameter of 50 μm, and the width of the main channel, where the worm is imaged, is 500 μm.

PDMS casts of the master employed a 10 : 1 base to curing agent ratio of Dow Sylgard™ 184 silicone elastomer, and cured overnight at 75 °C. Channel inlets and outlets were pierced into the cast PDMS *via* a 1 mm biopsy punch (Integra® Miltex). To deposit a thin layer of PDMS on the device substrate, 150–200 μL of 10 : 1 degassed PDMS were pressed between two 24 × 50 mm glass coverslips, which were then pulled apart to thinly coat both slides. This PDMS layer allows oxygen inhibition which prevents hydrogel bonding to the glass substrate during device operation. Cast devices were bonded pattern-down onto the coated substrate after partially curing the PDMS coating at 75 °C for 20 minutes. Devices were then fully cured at 75 °C for 3–4 hours.

Particle image velocimetry and analysis

To determine the instantaneous flow velocity at any point inside the microfluidic device, we adopted a particle image velocimetry approach. Calibration beads (SPHERO™ Rainbow) of 3.0–3.4 μm in diameter were mixed into the prepolymer solution at approximately 3200 particles μL^{-1} density. Beads flowing inside the microfluidic device were recorded for 5 seconds at 300 frames per second using a high-speed camera (Phantom® model v4.3) mounted on an inverted microscope (Leica DMI3000 B) with a 10× objective (0.3 NA). The images were pre-processed to visualize only the beads by taking the difference between each time frame and the average image of all frames. The pre-processed videos were inputted into PIVlab, an open-source MATLAB Particle Image Velocimetry tool. The calculated velocity vectors were averaged across all 1500 frames for the data in Fig. 2 and the first 500 frames before UV illumination for the data in Fig. 5.

Hydrogel size and crosslinking density characterization

The hydrogel prepolymer solution consisted of 10, 20, and 30% (v/v) poly(ethylene glycol) diacrylate (PEGDA700, Mn = 700 Da, Sigma-Aldrich), 10% (v/v) fluorescein *o*-acrylate (1 mg ml^{-1} in 1 M NaOH, Sigma-Aldrich), 10% (v/v) lithium phenyl-2,4,6-trimethylbenzoylphosphinate (LAP, 1.7 M in DI water, Sigma-Aldrich), and 70%, 60%, and 50% (v/v) DI water, respectively. Fluorescein *o*-acrylate was added to measure the fluorescence intensity of conjugated fluorescein as a proxy for hydrogel crosslinking density. Hydrogels were polymerized inside the PDMS device with UV exposure through a 200 μm diameter circular field diaphragm on a 10× objective at an intensity of 796 mW cm^{-2}. Images of the circular area of the hydrogel were taken in brightfield. For fluorescence imaging, the hydrogels were rinsed with DI water to remove unbound fluorescein. Hydrogel cross-sectional areas and fluorescence intensities were measured using the ImageJ software.

Simultaneous recoding of neuronal activity and behavior

Neuronal activities and concurrent behavior were recorded using an epifluorescence microscope (Leica DMI3000 B) with a color-selective light engine (Lumencor® SPECTRA X) and a two-channel camera (Hamamatsu ORCA-D2). The light wavelengths associated with the two-color fluorescence imaging and UV illumination are as follows: green (illumination: 485 nm; filter: 525 nm), red (illumination: 560

nm; filter: 617 nm), and UV (illumination 390 nm). A 10× objective was used.

The hydrogel prepolymer solution consisted of 30% (v/v) poly(ethylene glycol) diacrylate (PEGDA700, Mn = 700 Da, Sigma-Aldrich), 10% (v/v) fluorescein *o*-acrylate (1 mg ml^{-1} in 1 M NaOH, Sigma-Aldrich), 10% (v/v) lithium phenyl-2,4,6-trimethylbenzoylphosphinate (LAP, 1.7 M in DI water, Sigma-Aldrich), and 50% (v/v) DI water. To minimize hydrogel swelling with changes in the liquid environment in the device, the "buffer" solutions contained 20% (v/v) PEGDA700, and the chemical stimulus solution contained 20% (v/v) PEGDA700 and 1% (v/v) isoamyl alcohol (SAFC®) and several drops of blue food dye for brightfield and fluorescence validation of liquid delivery.

The *C. elegans* strain used for sparse multi-neuronal imaging is ZC3292 yxEx1701[glr-1p::GCaMP6s, glr-1p::NLS-mCherry-NLS].[38] The strain expresses cytosolic GCaMP and nuclear mCherry, driven by the *glr-1* promoter. For imaging, worms aged larval L4 to day^{-1} adult stage were loaded into the hub of a needle connected to the worm inlet channel. Gel polymerization and worm entrapment were performed as depicted in Fig. 1d. MATLAB scripts triggered a recording under green and cyan excitation light and alternately opened and closed solenoid-operated pinch valves (Cole-Parmer®) around the buffer and chemical stimulus tubing. Following imaging, worms and hydrogels were flushed from the device at 50–60 psi.

Analysis of imaging data

Neuron positions across time were tracked using the ImageJ TrackMate plugin on nuclear-localized fluorescence in red-channel recordings. Then, using the tracking data, a custom MATLAB script extracted the fluorescence intensity of each neuron across time in spatially registered red and green-channel recordings. For each frame in the recordings, the mean ("background") pixel intensity was subtracted from individual pixel intensities. Fluorescence intensity was calculated as the average of the top 20% background-normalized pixel intensities within a 3.5-pixel radius of the neuron center. For each neuron, the normalized ratio of green to red fluorescence, $\Delta R/R_0$, was calculated using the following formula, where R is the ratio of the neuron's green to red intensity in a single frame, and R_0 is the ratio of the neuron's mean green intensity to its mean red intensity across all frames:

$$\frac{\Delta R}{R_0} = \frac{R - R_0}{R_0}$$

To produce a kymograph of the worm motion, a binary mask of the worm body was isolated in ImageJ, taking advantage of the specimens' autofluorescence in green channel recordings. This mask was skeletonized to approximate the body centerline. Using MATLAB, the skeleton was fit to a 50-point smoothing spline. At each point n along the spline, the curvature was calculated as the reciprocal of the radius (in pixels) of a circle passing through the points $n - 2$, n, and $n + 2$.

Conflicts of interest

There are no conflicts to declare.

Acknowledgements

The authors acknowledge the funding support of the U.S. NIH (R01MH130064, R01NS115484, R01AG082039) to HL and the U. S. NSF (1764406) to HL. HL thanks C. Luthio for moral support.

References

1 K. M. Hallinen, R. Dempsey, M. Scholz, X. Yu, A. Linder, F. Randi, A. K. Sharma, J. W. Shaevitz and A. M. Leifer, *eLife*, 2021, **10**, e66135.
2 F. B. Shipley, C. M. Clark, M. J. Alkema and A. M. Leifer, *Front. Neural Circuits*, 2014, **8**, 28.
3 S. Faumont, G. Rondeau, T. R. Thiele, K. J. Lawton, K. E. McCormick, M. Sottile, O. Griesbeck, E. S. Heckscher, W. M. Roberts, C. Q. Doe and S. R. Lockery, *PLoS One*, 2011, **6**, e24666.
4 A. A. Atanas, J. Kim, Z. Wang, E. Bueno, M. Becker, D. Kang, J. Park, T. S. Kramer, F. K. Wan, S. Baskoylu, U. Dag, E. Kalogeropoulou, M. A. Gomes, C. Estrem, N. Cohen, V. K. Mansinghka and S. W. Flavell, *Cell*, 2023, **186**, 4134–4151.e31.
5 J. N. Stirman, M. M. Crane, S. J. Husson, S. Wabnig, C. Schultheis, A. Gottschalk and H. Lu, *Nat. Methods*, 2011, **8**, 153–158.
6 H. Ji, A. D. Fouad, Z. Li, A. Ruba and C. Fang-Yen, *Proc. Natl. Acad. Sci. U. S. A.*, 2023, **120**, e2219341120.
7 J. G. White, E. Southgate, J. N. Thomson and S. Brenner, *Philos. Trans. R. Soc., B*, 1986, **314**, 1–340.
8 S. Brenner, *Genetics*, 1974, **77**, 71–94.
9 N. Chronis, M. Zimmer and C. I. Bargmann, *Nat. Methods*, 2007, **4**, 727–731.
10 Y. Cho, S. A. Lee, Y. L. Chew, K. Broderick, W. R. Schafer and H. Lu, *Small*, 2020, **16**, 2070050.
11 S. Chaudhary, S. Moon and H. Lu, *Nat. Commun.*, 2022, **13**, 5165.
12 S. Kato, H. S. Kaplan, T. Schrödel, S. Skora, T. H. Lindsay, E. Yemini, S. Lockery and M. Zimmer, *Cell*, 2015, **163**, 656–669.
13 X. Zhan, C. Chen, L. Niu, X. Du, Y. Lei, R. Dan, Z.-W. Wang and P. Liu, *Nat. Commun.*, 2023, **14**, 4534.
14 A. Gordus, N. Pokala, S. Levy, S. W. Flavell and C. I. Bargmann, *Cell*, 2015, **161**, 215–227.
15 L. Luo, Q. Wen, J. Ren, M. Hendricks, M. Gershow, Y. Qin, J. Greenwood, E. R. Soucy, M. Klein, H. K. Smith-Parker, A. C. Calvo, D. A. Colón-Ramos, A. D. T. Samuel and Y. Zhang, *Neuron*, 2014, **82**, 1115–1128.
16 J. Larsch, S. W. Flavell, Q. Liu, A. Gordus, D. R. Albrecht and C. I. Bargmann, *Cell Rep.*, 2015, **12**, 1748–1760.
17 J. P. Nguyen, A. N. Linder, G. S. Plummer, J. W. Shaevitz and A. M. Leifer, *PLoS Comput. Biol.*, 2017, **13**, e1005517.

18 V. Venkatachalam, N. Ji, X. Wang, C. Clark, J. K. Mitchell, M. Klein, C. J. Tabone, J. Florman, H. Ji, J. Greenwood, A. D. Chisholm, J. Srinivasan, M. Alkema, M. Zhen and A. D. T. Samuel, *Proc. Natl. Acad. Sci. U. S. A.*, 2016, **113**, E1082–E1088.
19 C. Brunner, M. Grillet, A. Urban, B. Roska, G. Montaldo and E. Macé, *Nat. Protoc.*, 2021, **16**, 3547–3571.
20 J. D. Seelig, M. E. Chiappe, G. K. Lott, A. Dutta, J. E. Osborne, M. B. Reiser and V. Jayaraman, *Nat. Methods*, 2010, **7**, 535–540.
21 A. J. Barker and H. Baier, *Curr. Biol.*, 2015, **25**, 2804–2814.
22 Y. Cho, D. N. Oakland, S. A. Lee, W. R. Schafer and H. Lu, *Lab Chip*, 2018, **18**, 601–609.
23 S. Faumont, A. C. Miller and S. R. Lockery, *J. Neurobiol.*, 2005, **65**, 171–178.
24 S. Faumont and S. R. Lockery, *J. Neurophysiol.*, 2006, **95**, 1976–1981.
25 D. B. Dusenbery, *J. Comp. Physiol.*, 1980, **4**, 327–331.
26 K. E. McCormick, B. E. Gaertner, M. Sottile, P. C. Phillips and S. R. Lockery, *PLoS One*, 2011, **6**, e25710.
27 M. I. Prasanth, G. S. Santoshram, J. P. Bhaskar and K. Balamurugan, *Age*, 2016, **38**, 27.
28 X. Guo, P. Bian, J. Liang, Y. Wang, L. Li, J. Wang, H. Yuan, S. Chen, A. Xu and L. Wu, *Chem. Res. Toxicol.*, 2014, **27**, 990–1001.
29 S. S. Aykar, D. E. Reynolds, M. C. McNamara and N. N. Hashemi, *RSC Adv.*, 2020, **10**, 4095–4102.
30 C. Lee, C. D. O'Connell, C. Onofrillo, P. F. M. Choong, C. D. Bella and S. Duchi, *Stem Cells Transl. Med.*, 2020, **9**, 302–315.
31 D. Dendukuri, S. S. Gu, D. C. Pregibon, T. A. Hatton and P. S. Doyle, *Lab Chip*, 2007, **7**, 818–828.
32 D. Dendukuri, D. C. Pregibon, J. Collins, T. A. Hatton and P. S. Doyle, *Nat. Mater.*, 2006, **5**, 365–369.
33 K. W. Bong, D. C. Pregibon and P. S. Doyle, *Lab Chip*, 2009, **9**, 863–866.
34 V. Chan, P. Zorlutuna, J. H. Jeong, H. Kong and R. Bashir, *Lab Chip*, 2010, **10**, 2062–2070.
35 I. Rehor, S. van Vreeswijk, T. Vermonden, W. E. Hennink, W. K. Kegel and H. B. Eral, *Small*, 2017, **13**(39), 1701804.
36 H. Lee, Y. H. Roh, H. U. Kim and K. W. Bong, *Biomicrofluidics*, 2018, **12**, 054105.
37 A. San-Miguel and H. Lu, Microfluidics as a tool for *C. elegans* research, *WormBook*, ed. The C. elegans Research Community, WormBook, 2013, DOI: **10.1895/wormbook.1.162.1**, **https://www.wormbook.org**.
38 H. J. Lee, J. Liang, S. Chaudhary, S. Moon, Z. Yu, T. Wu, H. Liu, M.-K. Choi, Y. Zhang and H. Lu, *eLife*, 2023, DOI: **10.7554/elife.89050.1**.